Electronic Structure of Si-Doped BN Nanotubes Using X-ray Photoelectron Spectroscopy and First-Principles Calculation

Yong Jae Cho,[†] Chang Hyun Kim,[†] Han Sung Kim,[†] Jeunghee Park,*[,†] Hyun Chul Choi,[‡] Hyun-Joon Shin,[§] Guohua Gao,[#,||] and Hong Seok Kang*[,||]

Department of Chemistry, Korea University, Jochiwon, Chungnam 339-700, Korea, Department of Chemistry, Chonnam National University, Gwangju, Chonnam 500-757, Korea, Pohang Accelerator Laboratory and Department of Physics, Pohang University of Science & Technology, San 31 Hyojadong, Pohang 790-784, Korea, and Department of Nano and Advanced Materials, College of Engineering, Jeonju University, Chonju, Chonbuk 560-709, Korea

Received September 20, 2008. Revised Manuscript Received November 12, 2008

Silicon (Si)-doped multiwalled boron nitride nanotubes (BNNTs) were synthesized via thermal chemical vapor deposition. Electron energy-loss spectroscopy revealed that 5% of Si atoms were homogeneously doped into the BNNTs. X-ray absorption and photoelectron spectroscopy measurements demonstrated that the Si−B and Si−N bonding structures are produced, where both structures reduce the π bonding states of the BN sheets. The valence band analysis indicates that the Si doping decreases the band gap by about 1.7 eV. The first principles calculation of the Si-doped double-walled BNNTs suggests two distinctive doping structures; contiguous Si−Si bonding structures along the tube axis and a local hollow nitrogen-rich pyridine-like structure with a lone electron pair. It also predicts that the 4% Si-doped defective structures reduce the band gap of the BNNTs by 1.6 eV, which is in qualitative agreement with our experimental results.

1. Introduction

Since the discovery of carbon nanotubes (CNTs) in 1991,[1] extensive research has been conducted on novel analogous tubular structures, such as boron nitride nanotubes (BNNTs). Unlike CNTs, the band structure of BNNTs shows semiconducting properties with a nearly constant band gap (5.5 eV), which is weakly dependent on the tube diameter and chirality.[2−5] Therefore, the modification of their properties by doping has attracted a great deal of interest. Recent work has revealed that the band gap of BNNTs can be effectively tailored by carbon (C) doping, depending on their atomic compositions and configurations.[6−13] On the other hand, the doping of silicon (Si), which belongs to the same group as C, group IV, but strongly prefers sp^3-like bonding, is considered to influence the electronic and structural properties of CNTs and BNNTs in a different way from that of C doping.[14−20] Theoretically, it was predicted that the large outward displacement of the Si atom and its nearest-neighbor C atoms may impose changes in the chemical reactivity and, hence, in the interaction with foreign atoms and molecules through the Si sites.[14,15] A quadratic dependence of the band gap upon the Si concentration was also calculated for single-walled CNTs.[16] Unfortunately, no experimental reports of Si-doped CNTs have so far been published, which would allow the theoretical predictions to be confirmed.

For Si-doped BNNTs, a first-principle calculation showed that the incorporation of a Si atom into a B site of the single-

* Corresponding authors. E-mail: parkjh@korea.ac.kr; hsk@jj.ac.kr.
[†] Korea University.
[‡] Chonnam University.
[§] Pohang University of Science & Technology.
[||] Jeonju University.
[#] Permanent address: Pohl Institute of Solid State Physics, Tongji University, Shanghai 200092, P. R. China.

(1) Iijima, S. *Nature* **1991**, *56*, 354.
(2) Rubio, A.; Corkill, J. L.; Cohen, M. L. *Phys. Rev. B* **1994**, *49*, 5081.
(3) Chopra, N. G.; Luyken, R. J.; Cherrey, K.; Crespi, V. H.; Cohen, M. L.; Louie, S. G.; Zettl, A. *Science* **1995**, *269*, 966.
(4) Arenal, R.; Stephan, O.; Kociak, M.; Taverna, D.; Loiseau, A.; Colliex, C. *Phys. Rev. Lett.* **2005**, *95*, 127601.
(5) Wirtz, L.; Marini, A.; Rubio, A. *Phys. Rev. Lett.* **2006**, *96*, 126104.
(6) Liu, A. Y.; Wentzcovitch, R. M.; Cohen, M. L. *Phys. Rev. B* **1989**, *39*, 1760.
(7) Miyamoto, Y.; Rubio, A.; Cohen, M. L.; Louie, S. G. *Phys. Rev. B* **1994**, *50*, 4976.
(8) (a) Watanabe, M. O.; Itoh, S.; Sasaki, T.; Mizushima, K. *Phys. Rev. Lett.* **1996**, *77*, 187. (b) Chen, Y.; Barnard, J. C.; Palmer, R. E.; Watanabe, M. O.; Sasaki, T. *Phys. Rev. Lett.* **1999**, *83*, 2406.
(9) Blase, X.; Charlier, J.-C.; De Vita, A.; Car, R. *Appl. Phys. Lett.* **1997**, *70*, 197.
(10) Enyashin, A. N.; Makurin, Y. N.; Ivanovskii, A. L. *Carbon* **2004**, *42*, 2081.
(11) Wu, J.; Han, W.-Q.; Walukiewicz, W.; Ager III, J. W.; Shan, W.; Haller, E. E.; Zettl, A. *Nano Lett.* **2004**, *4*, 647.
(12) (a) Golberg, D.; Dorozhkin, P. S.; Bando, Y.; Mitome, M.; Tang, C. C. *Diamond Relat. Mater.* **2005**, *14*, 1857. (b) Wang, W. L.; Bai, X. D.; Liu, K. H.; Xu, Z.; Golberg, D.; Bando, Y.; Wang, E. G. *J. Am. Chem. Soc.* **2006**, *128*, 6530.
(13) Kim, S. Y.; Park, J.; Choi, H. C.; Ahn, J. P.; Hou, J. Q.; Kang, H. S. *J. Am. Chem. Soc.* **2007**, *129*, 1705.
(14) (a) Baierle, R. J.; Fagan, S. B.; Mota, R.; da Silva, A. J. R.; Fazzio, A. *Phys. Rev. B* **2001**, *64*, 085413. (b) Fagan, S. B.; Mota, R.; Baierle, R. J.; da Silva, A. J. R.; Fazzio, A. *Diamond Relat. Mater.* **2003**, *12*, 861. (c) Fagan, S. B.; da Silva, A. J. R.; Mota, R.; Baierle, R. J.; Fazzio, A. *Phys. Rev. B.* **2003**, *67*, 033405.
(15) Zhou, J.; Wang, C. *Chin. Sci. Bull.* **2005**, *50*, 1823.
(16) Avramov, P. V.; Sorokin, P. B.; Fedorov, A. S.; Fedorov, D. G.; Maeda, Y. *Phys. Rev. B.* **2006**, *74*, 245417.
(17) Guerini, S.; Kar, T.; Piquini, P. *Eur. Phys. J. B* **2004**, *38*, 515.
(18) Si, M. S.; Xue, D. S. *Europhys. Lett.* **2006**, *76*, 664.
(19) Griebel, M.; Hamaekers, J. *Comput. Mater. Sci.* **2007**, *39*, 502.
(20) (a) Xu, S.; Fan, Y.; Luo, J.; Zhang, L.; Wang, W.; Yao, B.; An, L. *Appl. Phys. Lett.* **2007**, *90*, 013115. (b) Fan, Y.; Wang, Y.; Lou, J.; Xu, S.; Zhang, L.; An, L.; Heinrich, H. *J. Am. Ceram. Soc.* **2006**, *89*, 740.

10.1021/cm802559m CCC: $40.75
Published on Web 12/09/2008

walled nanotubes has a relatively lower formation energy.[17] The pyrolysis synthesis of Si (∼6%)-doped bamboolike multiwalled BNNTs was recently reported by An and coworkers.[20] Nevertheless, the electronic states, especially the state-resolved distributions of the compositional elements, have not been experimentally scrutinized in order to address the role of Si doping in the atomic arrangement as well as in the band gap.

In the present work, we synthesized 5% Si-doped multiwalled (MW) BNNTs by the thermal chemical vapor deposition (CVD) method and performed systematic analytical investigations of the electronic structures of the nanotubes using synchrotron X-ray photoelectron spectroscopy (XPS) and the X-ray absorption near edge structure (XANES) method. We also estimated their band gap using the XPS valence band spectra. To gain further insight into the electronic structures of the synthesized Si-doped BNNTs, we investigated various isomers of double-walled (DW) BNNTs using the first principles method, particularly of (12,0)@(20,0) BNNT. The results show that the relative stabilities of the isomers are sensitive to the arrangement of the Si atoms. To the best of our knowledge, this is the first time that the electronic structures of Si-doped BNNTs have been investigated by both experimental and theoretical methods.

2. Experimental Section

B pieces (99%, MaTeck) and BN (99%, Aldrich) powder were ball-milled separately for 20 h, using a mechanical ball mill system (Spex 8000M). These ball-milled powders and a piece of Si wafer were placed in an alumina boat inside a quartz tube reactor. Alumina substrates were coated with an ethanol solution of $FeCl_2 \cdot 4H_2O$ (99%, Aldrich), producing Fe nanoparticles deposited on the substrates. These substrates were used to cover the boat containing the source. Ammonia gas was introduced into the quartz tube when the temperature reached 1200 °C. After 2 h of growth, a white colored product was observed to be deposited homogeneously over a large area of the substrates. The size, structure, and composition of the product were examined by SEM (Hitachi S-4300), field-emission TEM (FEI TECNAI G^2 200 kV and Jeol JEM 2100F), EELS (GATAN GIF-2000) in conjunction with TEM (TECNAI G^2), and Raman spectroscopy (Renishaw 1000) using the 514.5 nm line of an argon ion laser.

The XPS measurements were performed at the U7 beam line of the Pohang Light Source (PLS). Briefly, the XPS data were collected using photon energies in the range of 360−1265 eV, with a photon flux within the range of 7×10^{11} to 3×10^{10} (photons/s/200 mA). The binding energies were corrected for specimen charging by referencing the C 1s peak to 284.6 eV. The experiment was performed in an ultrahigh vacuum (UHV) chamber with a base pressure $\leq 5 \times 10^{-10}$ Torr. The energy of the photoelectrons emitted from the surface of the nanotubes was analyzed with an electron energy analyzer (Physical Electronics model PHI 3057 with a 16-channel detector). The analyzer was located at an angle of 55° from the surface normal. The B and N K-edges XANES measurement was also performed at the same beam line. The spectral resolving power ($E/\Delta E$) of the incident photons is about 5000 at 400 eV. The angle of the incident X-ray beam to the sample plane was tuned from 15 to 90°. All of the spectra were taken in total electron yield mode in which the sample current was recorded at room temperature.

Total energy calculations were carried out using the Vienna ab initio simulation package (VASP).[21] The electron-ion interactions were described by the projected augmented wave (PAW) method,[22] which is basically a frozen-core all-electron calculation. The exchange-correlation effect was treated within the local density approximation (LDA), because it reproduces the interlayer interactions of graphite and *h*-BN correctly. We adopt a supercell geometry in which *k*-space sampling is done with an appropriate number of *k*-points in the irreducible region of the first Brillouin zone along the tube axis, depending upon the size of the supercell. In doing this, we use large supercells, which guarantee that the interatomic distances between neighboring cells are greater than 7.00 Å. The cutoff energy is set high (= 400 eV) enough to ensure accurate results, and the conjugate gradient method is employed to optimize the geometry until the Hellmann−Feynman force exerted on an atom is less than 0.03 eV/Å. Our calculations are based on optimized zigzagged (12,0)@(20,0) and (7,0)@(15,0) DW BNNTs. This is because Golberg et al. reported that most MW BNNTs have preferentially zigzag [(*n*,0) type] chirality along their circumference, based on their electron diffraction patterns.[23] We note that these two DW BNNTs show the most favorable binding between the inner and outer shells among the (*n*,0)@(20,0) and (*n*,0)@(15,0) BNNTs.[24]

3. Results and Discussion

3.1. Morphology and Composition: SEM, TEM, and EELS. Figure 1a shows the SEM image for the Si-doped BNNTs grown on the substrates. Their length is in the range of 40−50 μm. The surface is periodically bumpy over the entire nanotubes. The inset shows clearly the hollow inside of the nanotubes. The TEM image shows a typical morphology consisting of a bamboo-like structure in which the inside of the nanotubes is separated by a series of compartment layers (Figure 1b). The average diameter of the nanotubes is 150 nm, and roundly curved compartment layers appear periodically with a distance (between them) of 300 nm. The lattice-resolved TEM image for the edge of the wall part, shows the (002) basal planes aligned along the tube axis, with a high degree of crystalline perfection (Figure 1c). The spots in the fast Fourier-transformed electron diffraction (FFT ED) pattern can be indexed as the (002) basal planes of the *h*-BN layers (inset).

Figure 1d shows the EELS elemental distribution of the B, N, Si, and O atoms over the whole nanotube, showing the homogeneous distribution of Si and the thin oxide outerlayers. Its corresponding EELS spectrum is displayed in Figure 1e. The inset shows the magnified Si peak after background subtraction. For all parts, the average value of the Si concentration, defined as the [Si]/([B] + [N] + [Si]) atomic ratio, was found to be uniformly about 0.05 (with 10% uncertainty) using software (DigitalMicrograph for GMS1.2, Gatan Inc.). The spectrum shows two distinct absorption features corresponding to the known K-shell ionization edges of the B and N atoms starting from around 186 and 396 eV, respectively. The sharply defined 1s → π^*

(21) (a) Kresse, G.; Hafner, J. *Phys. Rev. B* **1993**, *47*, 558. (b) Kresse, G.; Furthmüller, J. *Phys. Rev. B* **1996**, *54*, 11169.
(22) Kresse, G.; Joubert, D. *Phys. Rev. B* **1999**, *59*, 1758.
(23) Golberg, D.; Bando, Y.; Kurashima, K.; Sato, T. *Solid State Commun.* **2000**, *116*, 1.
(24) Okada, S.; Saito, S.; Oshiyama, A. *Phys. Rev. B* **2002**, *65*, 165410.

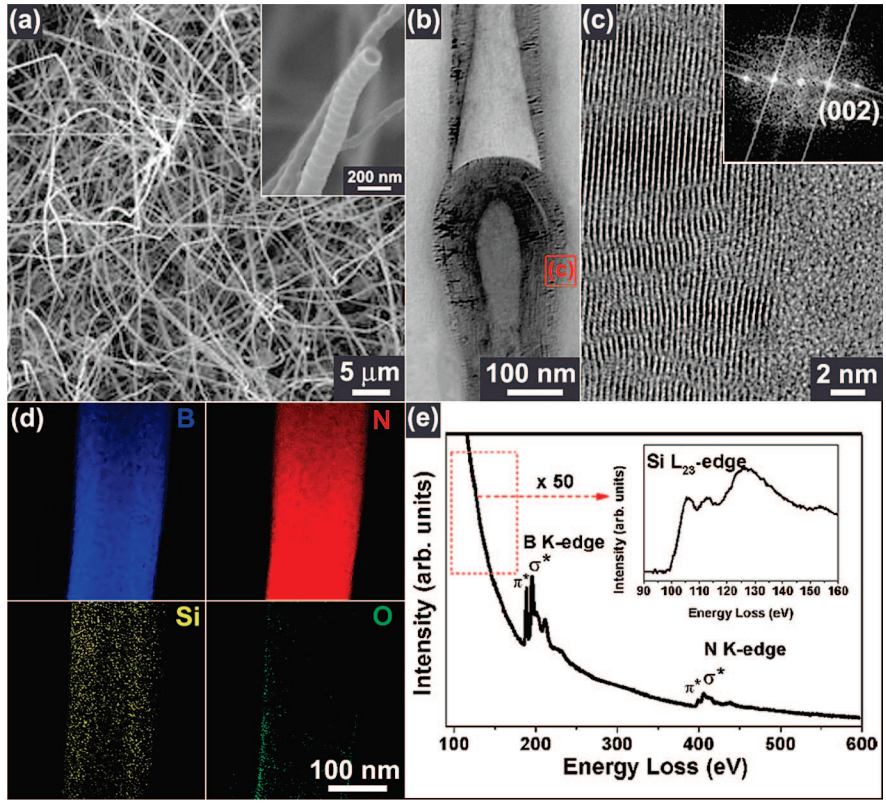

Figure 1. (a) SEM micrograph showing the high-density Si-doped BNNTs grown on the substrates and their periodically bumpy surface and hollow inside (inset). (b) TEM image showing a bamboo-like structure. (c) Lattice-resolved TEM image for the edge part of the wall layers with its corresponding FFT ED pattern (inset). (d) EELS mapping of B, N, Si, and O atoms, and (e) its corresponding spectrum. The EELS spectrum shows two distinct absorption features starting at around 186 and 396 eV, corresponding to the known K shell edges for B and N, respectively. The inset shows the background-subtracted Si L_{23}-edge peak, with an onset at 99 eV.

(at 188 eV for B and 399 eV for N) and broad 1s → σ^* transition features indicate that the nanostructures are still composed of sp^2 hybridized *h*-BN sheets. The L_{23}-shell ionization edge of the Si atoms starts from 99 eV and shows two distinctive peaks at about 106 and 113 eV, corresponding to the 2p → p* and 2p → d* transitions, respectively, and a third prominent broad peak separated from the first peak by about 20 eV. At first sight, the spectrum looks very similar to that of SiO_2.[25] However, there are differences in their peak onsets, starting at a lower energy (99 eV) than that of SiO_2 (104 eV), and in the peak width, which is broadened in the case of the BNNTs. This feature can be ascribed to the bonding of the Si atoms with the B or N atoms (in the *h*-BN sheets), which are less electronegative than the O atoms.

3.2. XPS and XANES: Electronic Structure of B, N, and Si atoms. We measured the survey-scanned XPS spectra of the undoped and Si-doped BNNTs (see the Supporting Information, Figure S1). The relative ratios of the B, N, and Si atoms were estimated from the area ratios of the B 1s, N 1s, and Si 2p peaks, respectively, and the sensitivity factors. The Si content remained constant at 0.08 ± 0.05. To probe the electronic structures of the individual atoms, we measured their fine-scanned spectra, as shown in Figure 2. For comparison, the fine-scanned peaks of the undoped BNNTs and the Si_3N_4 powder were measured. Figure 2a shows the B 1s spectra of the BNNTs and Si-doped BNNTs, measured using 625 eV. The band can be deconvoluted into three bands at 189.1 (PB0), 191.2 (PB1), and 192.3 (PB2) eV, respectively. The electronegativity difference of the elements suggests that the binding energy of the B−Si structures would be lower than that of B−N, whereas that of the B atoms bonded to dangling bonds or defects (usually bonded to more electronegative O atoms) would be higher. Therefore the PB0, PB1, and PB2 bands can be assigned to the B−Si, B−N, and B−O bonding structures, respectively. The width and area % values of the three resolved bands are listed in Table 1. The average area % values of the PB0, PB1, and PB2 bands are 35, 45, and 20, respectively.

Figure 2b shows the N *1s* spectra of the Si-doped BNNTs, BNNTs, and Si_3N_4 powder. The band has been deconvoluted into three bands at 395.7 (PN0), 397.7 (PN1), and 399.0 (PN2) eV, respectively. Referring to the peak assignment of the BNNTs and Si_3N_4 powder and the electronegativity of elements (χ_P = 2.04 for B and χ_P = 1.90 for Si), the PN0 and PN1 bands can be assigned to the N atoms in the N−Si and N−B structures, respectively. According to the previous work done on BCN NTs, the highest-energy PN2 band can be ascribed to the dangling N atoms at defective hollow pyridine-like N−B or N−Si bonding structures (as suggested in section 3.4).[13] The average area % values of the PN0, PN1, and PN2 bands are 25, 40, and 35, respectively (Table 1). The two broad PN0 and PN2 bands of the Si_3N_4 powder at 397.5 and 399.3 eV, respectively, are ascribed to the N bonding with the Si and O(−Si) atoms.

(25) Egerton, R. F. *Electron Energy-Loss Spectroscopy in the Electron Microscope*, 2nd ed.; Plenum Press: New York, 1996.

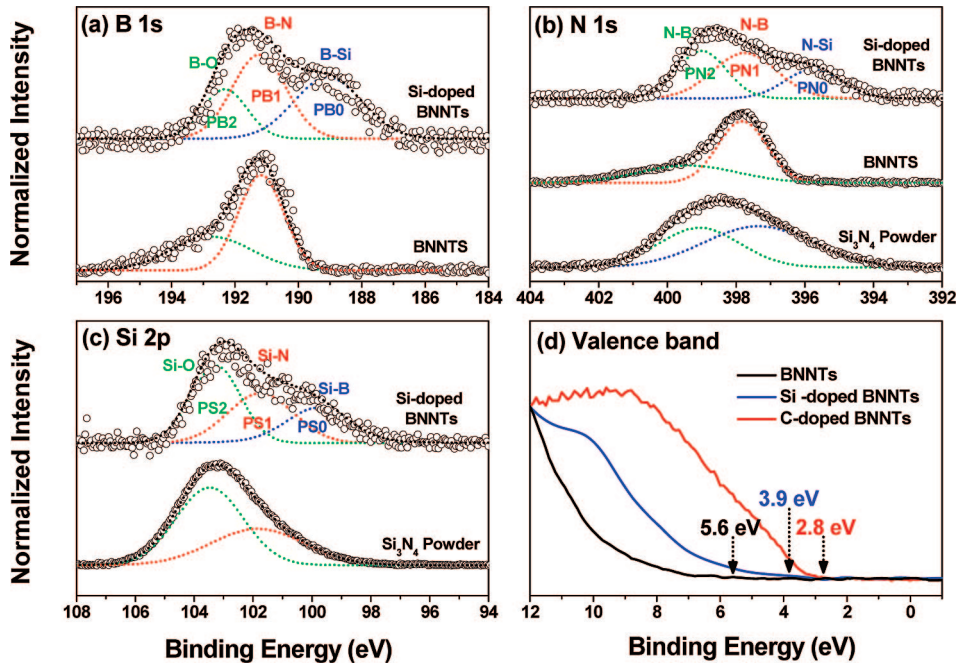

Figure 2. (a) B 1s XPS spectra of the BNNTs and Si-doped BNNTs, using 625 eV. The data points (open circles) of the B 1s band are fitted by three Voigt functions, PB0, PB1, and PB2 (dotted lines). (b) The N 1s XPS spectra of the Si_3N_4 powder, BNNTs, and Si-doped BNNTs. The data points (open circles) of the N 1s band are fitted by three Voigt functions, PN0, PN1, and PN2 (dotted lines). (c) The Si 2p XPS spectra of the Si_3N_4 powder and Si-doped BNNTs. The data points (open circles) of the Si 2p band are fitted by three Voigt functions, PS0, PS1, and PS2 (dotted lines). (d) XPS valence band spectrum using 240 eV for the BN NTs, $B_{0.45}C_{0.1}N_{0.45}$ NTs (10% C-doped BNNTs), and Si-doped BNNTs.

Table 1. Area % Values of the Deconvoluted Bands from the XPS B and N 1s Peaks, and Si 2p Peak for the Si-Doped BNNTs, Undoped BNNTs, and Si_3N_4 Powder

sample	element	band	bonding structures	position (eV)	width (eV)	area %
Si-doped BNNTs	B	PB0	B−Si	189.1	2.5	35
		PB1	B−N	191.2	2.0	45
		PB2	B−O	192.3	1.7	20
	N	PN0	N−Si	395.7	1.9	25
		PN1	N−B	397.7	2.2	40
		PN2	Pyridine-like N−B or N−Si	399.0	1.7	35
	Si	PS0	Si−B	99.8	2.6	25
		PS1	Si−N	101.7	2.6	35
		PS2	Si−O	103.3	2.0	40
BNNTs	B	PB1	B−N	191.0	1.8	55
		PB2	B−O	192.2	2.5	45
	N	PN1	N−B	397.8	1.7	65
		PN2	N−O	399.4	3.4	35
Si_3N_4 powder	N	PN0	N−Si	397.5	2.7	60
		PN2	N−O	399.3	2.8	40
	Si	PS1	Si−N	101.8	3.7	40
		PS2	Si−O	103.5	2.7	60

Figure 2c displays the Si *2p* spectra of the Si-doped BNNTs and Si_3N_4 powder. These spectra can be deconvoluted into three bands at 99.8 (PS0), 101.7 (PS1), and 103.3 (PS2) eV, respectively. The binding energy of the Si atoms bonded to the B, N, and O atoms would be expected to follow the order, Si−B < Si-*N* < Si−O, as predicted from the electronegativity differences. Therefore, the PS0, PS1, and PS2 bands can be assigned to the Si−B, Si−N, and Si−O bonding structures, respectively. The PS2 band would mainly originate from the SiOx outerlayers. The average area % values of the PS0, PS1, and PS2 bands are 25, 35, and 40, respectively (Table 1). This result indicates that the Si−N bonding structure is dominant over the Si−B bonding structure, which is consistent with the previous theoretical prediction.[17] The PS1 and PS2 bands of the Si_3N_4 powder at 101.8 and 103.5 eV, respectively, are assigned to the Si−N and Si−O bonding structures.

To investigate the nature of the band structure, we obtained the valence band (VB) emission spectrum using a photon energy of 240 eV. Figure 2d displays the XPS valence band spectra in the range of 0−12 eV for the BNNTs, Si-doped BNNTs, and 10% C-doped BNNTs ($B_{0.45}C_{0.1}N_{0.45}$ NTs, obtained from the data of ref.[13]). The spectra are normalized using the peak intensity at 12 eV. The zero energy is chosen at the Fermi level, E_f, which is calibrated using the threshold energy of gold foil. According to our previous study of BNNTs, the emission feature between 3.5 and 11 eV is mainly due to the B−N 2p π-bond electrons.[13] The corresponding σ-bond electrons determine the feature between 11 and 13 eV. The Si-doped BNNTs exhibit a significant intensity in the range of 3.5−10 eV, compared to the BNNTs, which is probably due to the increased density of states (DOS) of the Si−N structures. The positions of the valence band maximum relative to the Fermi level were evaluated by taking the onset of the valence band emission, and were found to be 5.6 and 3.9 eV for the BNNTs and Si-doped BNNTs, respectively. We estimated the band gap decrease of 1.7 eV caused by the Si doping from their unambiguous onset. For comparison, the spectrum of 10% C-doped BNNTs is also displayed, showing a more significant band gap decrease compared to the case of Si doping.[13]

The B and N K-edges XANES spectra were measured from the BNNTs and Si-doped BNNTs, at an incident angle

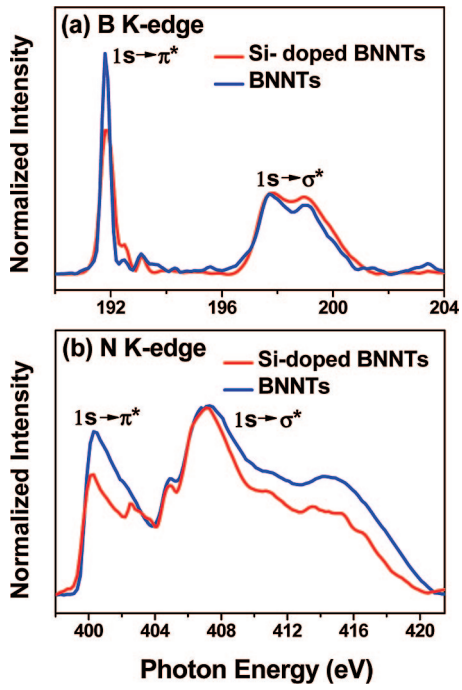

Figure 3. XANES spectra of the (a) B K-edge and (b) N K-edge of BNNTs and Si-doped BNNTs.

of 45°. In the B K-edge spectrum, the sharp absorption feature at 191.8 eV is due to the B 1s → π^* ($2p_z$) transition, showing a clear fingerprint of sp^2 hybridization (Figure 3a). The broad absorption features above 197 eV can be assigned to the B 1s → σ^* ($2p_{x,y}$) transition. The N K-edge spectrum is composed of the N 1s → π^* transition ($2p_z$) at 400.6 eV and the two major peaks corresponding to the N 1s → σ^* transitions ($2p_{x,y}$) at 407 and 415 eV, respectively, as shown in Figure 3b. It is important to note that the intensity ratio of the π^*/σ^* features of the Si-doped BNNTs is much lower than that of the BNNTs. We suggest that the incorporation of Si into the *h*-BN sheets significantly decreases the π bonding states by forming the Si−B and Si−N σ-bonding structures and pyridine-like structures.

3.3. Raman Spectroscopy. The Raman spectra of the BNNTs and Si-doped BNNTs show peaks at 1376 and 1371 cm^{-1}, respectively, corresponding to the *h*-BN Raman active mode, E_{2g}, derived from the in-plane atomic displacement of the B and N atoms toward each other (Figure 4).[26] The incorporation of Si atoms induces a lower-frequency shift of 5 cm^{-1}. The larger size of the Si dopants could cause an increase in the average bond length, thus leading to a significant softening effect. The full-width at half-maximum (fwhm) of the Si-doped BNNTs is 30 cm^{-1}. This result is consistent with that reported by An and co-workers.[20] The present BNNTs show a larger fwhm (38 cm^{-1}) than that (13 cm^{-1}) reported by other research groups, because of their defective N-rich BN layers.[27,28] The substitution of Si atoms would reduce the number of such defect sites, resulting in a narrower peak width.

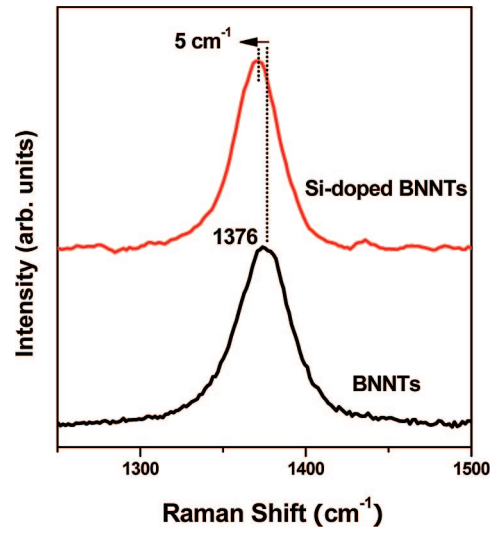

Figure 4. Raman spectra of the BNNTs and Si-doped BNNTs measured at room temperature. The excitation wavelength is 514.5 nm.

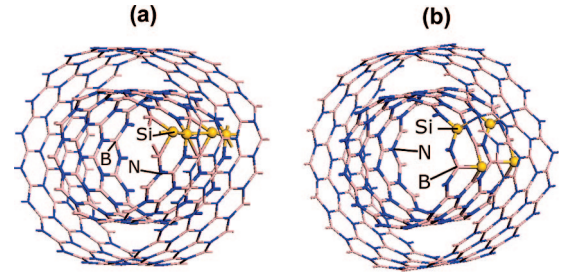

Figure 5. (a) Isomer A_2 and (b) isomer B_2 of the (12,0)@(20,0) DW BNNT, in which one B and one N atom are doped in the inner shell. For a better understanding, two primitive cells are shown.

3.4. First-Principles Calculation on Si-Doped DW BNNT Isomers. We investigated the topology and electronic structures of the Si-doped DW BNNTs using first-principles calculations, based on the experimental data showing that (1) the multiwalls of the BNNTs are doped homogeneously with 5% Si atoms; (2) the Si−N bonding structure is dominant over the Si−B bonding structure; (3) the hollow pyridine-like structure can be formed; (4) the Si doping decreases the π-bond bonding structures of h-BN sheets; (5) the band gap decreases by 1.7 eV upon the 5% Si doping.

In the first step, we consider the simplest structure wherein the numbers of Si_B and Si_N atoms are the same, and select a particular doping of two Si atoms only on the inner shell of a (12,0)@(20,0) BNNT, in which one B and one N atom are substituted by Si atoms. We refer to this as the "*1*Si_B-1Si_N" doping structure, where the Si atoms substituted for the B and N atoms are denoted as Si_B and Si_N, respectively. For this calculation, we used eleven *k*-points in the first Brillouin zone of the primitive cell of the tube for *k*-point sampling, whose optimal lattice parameter was 4.3 Å. A primitive cell contains 48 and 80 atoms in the inner and outer shells of a (12,0)@(20,0) BNNT, respectively. Structures a and b in Figure 5 display those of the two most stable isomers, Isomers A_2 and B_2, respectively. Isomer A_2, in which the Si atoms form a contiguous row along the tube axis, is significantly more stable than the other isomers, and is 2.79 eV more stable than the second most stable isomer (isomer B_2), indicating that isomer A_2 will be exclusively

(26) Nemanich, R. J.; Solin, S. A.; Martin, R. M. *Phys. Rev. B* **1981**, *23*, 6348.
(27) Choi, H. C.; Bae, S. Y.; Jang, W. S.; Park, J.; Song, H. J.; Shin, H. J. *J. Phys. Chem. B* **2005**, *109*, 7007.
(28) Zhi, C.; Bando, Y.; Tang, C.; Golberg, D.; Xie, R.; Sekigushi, T. *Appl. Phys. Lett.* **2005**, *86*, 213110.

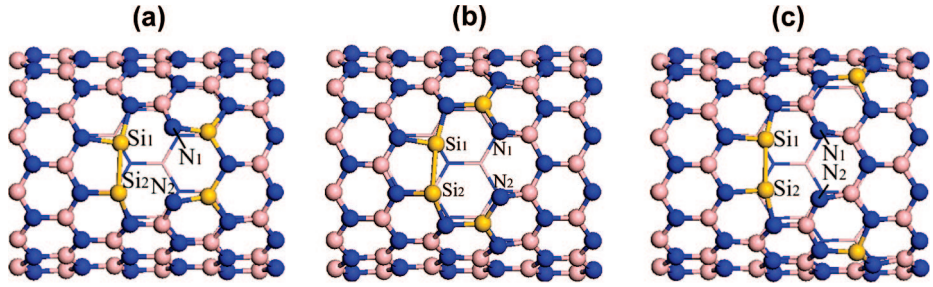

Figure 6. (a) Isomer α, (b) isomer β, and (c) isomer γ of the [$4Si_B$-X_{BN}]-doped (12,0) SW BNNT. See the text for the meaning of the doping pattern $4Si_B$-X_{BN}.

formed in the doping process. This result is consistent with a recent work on the BN-doped CNTs, showing that the total energy with an adjacent B/N atom pair is lower than those with separately doped B an N atoms at different position.[29] It is also noteworthy that the most stable isomer A_2 contains the Si−B bond mediated by Si−Si bonds, although the isolated Si−B bonds may be unstable. This rationalizes the Si−B bonding structures that are evidenced by XPS and XANES.

Henceforth, all our descriptions of $1Si_B$-$1Si_N$ doping will focus on isomer A_2. A similar calculation was also carried out for the $1Si_B$-$1Si_N$ doping of a (7,0)@(15,0) BNNT. We observed that it is much easier to dope the inner shell of the smaller diameter DW BNNTs than that of the larger diameter ones. Namely, the energy change, ΔE (DW BNNT + $2Si_i$), of doping of the inner shell, defined by the process DW BNNT + 2Si → $2Si_i$-doped DW BNNT + B + N for the (7,0)@(15,0) BNNT, is 0.97 eV smaller than that for the (12,0)@(20,0) BNNT [Here, the label "Si_i" indicates that the Si atoms are doped in the inner shell of the DW BNNT. In the meantime, we adopt the atomic energies for the chemical potentials of the Si, B, and N atoms]. This observation indicates that the $1Si_B$-$1Si_N$ doping could be initiated at the innermost shell of the MW BNNTs.

In isomer A_2, the Si_N protrudes from the circumference of the tube more significantly compared to Si_B, so that the Si_N-Si_B bond lengths are close to that of a single bond.[30] To clarify this, only the inner wall of the two isomers is displayed in the Supporting Information, Figure S2. There are two kinds of Si−Si bonds along the tube axis; one is a direct bond between adjacent Si atoms along the tube axis, whose bond length is 2.16 Å, and the other is the bond between those atoms which are diagonal to each other in a hexagon, whose bond length (= 2.26 Å) is slightly longer [Note that there is no such bond between the B and N atoms before the substitution]. As a result, the bond angles between the three Si atoms along the tube axis deviate from 180° by an appreciable degree, which amounts to 156.5 and 153.3° for the (7,0)@(15,0) and (12,0)@(20,0) BNNTs, respectively. The sp^2 network of proximal atoms is less disturbed for the doping of the smaller diameter DW BNNTs, which makes the doping easier. This appreciable degree of deformation in the tube rings makes the circular geometries of the shells become ellipsoid. However, as the diameter becomes much larger (i.e., the experimentally observed diameter of 200 nm), we would expect this ellipticity to become negligibly smaller.

Once the inner shell is doped, the subsequent doping of the same pattern is easier on the outer shell of the DW BNNTs. For example, the energy change, ΔE [$2Si_i$-(12,0)@(20,0) BNNT+$2Si_o$], for the doping of the outer shell, defined by the process DW $2Si_i$-BNNT + 2Si → DW $2Si_i$-$2Si_o$-BNNT + B + N for the (12,0)@(20,0) BNNT, is 0.97 eV more favorable than the first doping in the inner shell. In addition, we also find that the consequent doping of the outer shell (of DW BNNTs) is 0.58 eV more favorable than the corresponding doping of the (20,0) SW BNNT. These observations predict that the $1Si_B$-$1Si_N$ doping can propagate favorably to the outer shells, once initiated in the inner shell.

Next, we investigate the "$4Si_B$-X_{BN}" doping structure, in which a pair of BN atoms in the supercell is deleted first, followed by the substitution of four B atoms by Si atoms. Three primitive cells of zigzag BNNTs were taken as a supercell. We recall that Zobelli et al. recently showed that point defects forming under electron irradiation in BNNTs are primarily divacancies originating from the deletion of a pair of BN atoms.[31] For this doping pattern, we consider three isomers, α, β, and γ, as shown in Figure 6. They are characterized by two pyridine-like local structures around the site where a BN pair was deleted. These structures would be responsible for the pyridine-like B−N bonding structures (PN2 band of N 1s band). Two Si atoms (Si_1 and Si_2) are bonded to each other with bond lengths 2.40 Å, 2.45 Å, and 2.23 Å for isomers α, β, and γ, respectively, which is comparable to that (= 2.35 Å) of a Si−Si single bond.[30] The respective bond lengths of (Si_1−N_1, Si_2−N_2) are (2.54, 2.47), (3.05, 3.02), and (2.39 and 2.40) in Å units in three isomers. These distances are much larger than that (= 1.71 Å) in the Si−N single bond,[32] indicating that there is no Si−N bond in these isomers. Therefore, N_1 and N_2 are expected to have lone-pair electrons. In fact, our separate calculation for the molecule, $N_3B_2SiH_5$, shows that it has a planar geometry and its HOMO corresponds to the lone-pair state of the atom N_1, as shown in the Supporting Information, Figure S3. For the (12,0) BNNT, we find that isomer α is 0.68 and 2.96 eV more stable than isomers β and γ, respectively. Therefore, isomer α can be produced exclusively in these pyridine-like doping patterns. Although

(29) Xu, Z.; Lu, W.; Wang, W.; Gu, C.; Liu, K.; Bai, X.; Wang, E.; Dai, H. *Adv. Mater.* **2008**, *20*, 3615.
(30) Huheey, J. E.; Keiter, E. A.; Keiter, R. L. *Inorganic Chemistry*; Harper Collins College Publishers: New York, 1993; p A-31.
(31) Zobelli, A.; Ewels, C. P.; Gloter, A.; Seifert, G.; Stephan, O.; Csillag, S.; Colliex, C. *Nano Lett.* **2006**, *6*, 1955.
(32) Si−N bond lengths are in the range of 1.70−1.77 Å in crystalline Si_3N_4. See: Grun, R. *Acta Crystallogr. Sect. B* **1979**, *35*, 800; our LDA calculation also shows that the Si−-N bond length in the molecule SiH_3−NH_2 is 1.71 Å.

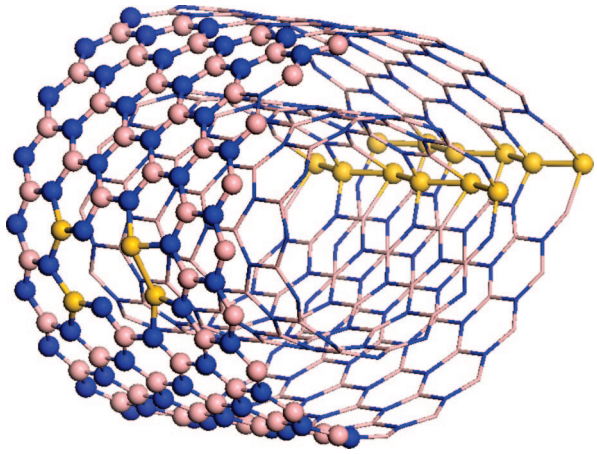

Figure 7. Molecular structure of $(4Si_B\text{-}X_{BN})_o\text{-}2Si_i\text{-}2Si_o$-(12,0)@(20,0) DW BNNT. See the text for the meaning of the doping pattern.

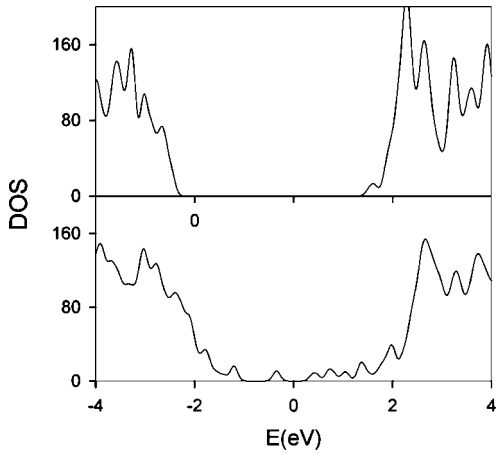

Figure 8. Electronic density of states for the (a) pristine (12,0)@(20,0) BNNT and (b) $(4Si_B\text{-}X_{BN})_o\text{-}2Si_i\text{-}2Si_o$-(12,0)@(20,0) BNNTs.

not explicitly shown here, other isomers, in which the Si atoms are doped in other six-member rings, are at least as unstable as isomer γ. It is also worth mentioning that there is no appreciable deformation along the circumference of the circular tube geometry, which is certainly different from the case of $1Si_B\text{-}1Si_N$ doping.

Finally, we consider the combination of two doping patterns in the DW BNNTs, as a model for 4% Si atoms homogeneously doped into BNNTs. We take three primitive cells of (12,0)@(20,0) BNNTs as a supercell. Figure 7 shows that $2Si_i-2Si_o-$BNNT is formed first by a sequence of $1Si_B\text{-}1Si_N$ doping into the inner and outer shells of the tube. In fact, six Si atoms, not two Si atoms, are doped in both shells along the tube axes, because a supercell contains three primitive cells. Then, the process of $4Si_B\text{-}X_{BN}$ doping at the outer shell introduces nitrogen-rich and pyridine-like defects to form the $(4Si_B\text{-}X_{BN})_o\text{-}2Si_i\text{-}2Si_o$-BNNT. This 4% Si doping in both the inner and outer shells closely resembles the homogeneous 5% Si doping of the synthesized BNNTs, as described above.

Figure 8 shows that this combined doping structure reduces the band gap significantly from that (~1.9 eV) of the pristine (12,0)@(20,0) BNNT to 0.3 eV, because of the introduction of many defect states around the Fermi level.[33] This decrease in the band gap is qualitatively consistent with our analysis of the XPS valence band spectra. Note that the actual band gap is very sensitive to the doping pattern, so the heteroatom doping can be a promising way of utilizing the BNNTs for semiconductor devices. Unfortunately, we could not consider the doping structures of the larger diameter MW BNNTs (practically beyond the present day computational limit), which would allow the electronic structures around the Fermi level to be determined. Furthermore, in the MW BNNTs, there can be other kinds of local structures containing Si atoms, which could possibly influence the electronic structures. For example, Si atoms may form small clusters in the interwall region. Nevertheless, we believe that this systematic study of the characteristics of Si-doped DW BNNTs is of great importance both for the furthering of their utilization and the development of suitable fabrication methods.

4. Conclusions

Five percent Si-doped MW BNNTs were synthesized via the thermal CVD of B/BN/Si powder under NH_3 flow at 1200 °C. They have a bamboo-like structure with an average diameter of about 150 nm. The EELS and XPS data reveal the existence of homogenously doped 5% Si atoms and SiO_x outerlayers. The band deconvolution of the fine-scanned XPS B 1s, N *1*s, and Si 2p peaks reveals the presence of a significant amount of Si−B and N−Si binding structures, where the Si−N bonding structure (Si_B doing) is dominant. The Si doping drastically decreases the π bonding states of the B and N atoms. From the XPS valence band spectra, the band gap decrease was estimated to be 1.7 eV.

Using the first-principles method based on DFT theory, we calculated the total energy of the various possible isomers of the Si-doped BNNTs, particularly of (12,0)@(20,0) DW BNNT. The "$1Si_B\text{-}1Si_N$" doping structure exhibits a strong tendency for the Si atoms to be doped contiguously along the tube axis, and for the propagation favorably to the outer shells, once initiated in the inner shell. As a model for pyridine-like hollow local structures with lone-pair electrons, we proposed a unique "$4Si_B\text{-}X_{BN}$" doping structure in which a pair of BN atoms is first deleted, followed by the substitution of B atoms by Si atoms. A combination of these two doping structures was suggested as one possible way of achieving the 4% homogeneous doping, in which the Si−N bond is dominant over the Si−B bond. The reduction of the band gap (1.6 eV) is in qualitative agreement with our experimental results. We believe that the present experimental and theoretical studies of Si-doped BNNTs will lead to a better understanding of the electronic structure of BN nanostructures, which is prerequisite to their application as nanoelectronic devices.

Acknowledgment. This work was supported by KRF grants (KRF-2008-314-C00175), KOSEF (R01-2008-000-10825-0;

(33) It is well known that the LDA underestimates the bandgap. This is the major reason why the band gap (= 1.9 eV) of the pristine (12,0)@(20,0) BNNTs is significantly smaller than that (= 5.6 eV) of the MW BNNTs experimentally observed in this work. However, it should also be noted that the gap decreases with increasing curvature of the tube. DW BNNTs with diameters much larger than those for the (12,0)@(20,0) tube can have a significantly larger band gap. A similar argument holds for Si-doped BNNTs.

M1080300121808), and MKE under the ITRC support program supervised by the IITA (IITA-2008-C1090-0804-0013). The SEM, HVEM, XRD, and XPS measurements were performed at the KBSI in Seoul, Daejeon Taegu, and Pusan, respectively. The experiments at the PLS were partially supported by MOST and POSTECH. H.S.K. is grateful to Jeonju University for its financial support. We also acknowledge the support from KISTI (Korea Institute of Science and Technology Information) under the 11th Strategic Supercomputing Applications Support Program. The use of the computing system of the Supercomputing Center is also greatly appreciated. H.C.C acknowledges the support from the KRF Grant (KRF-2008-331-C00192) funded by the Korean Government (MOEHRD, Basic Research Promotion Fund). H.-J.S. acknowledges the support from the KOSEF NCRC Grant (R15-2008-006-03002-0) funded by the Korean Government (MEST).

Supporting Information Available: Survey-scanned XPS spectra and various molecular structures related to the Si-doped BNNTs (PDF). This material is available free of charge via the Internet at http://pubs.acs.org.

CM802559M